

A year-long AGILE observation of Cygnus X-1 in hard spectral state

E. Del Monte¹, M. Feroci¹, Y. Evangelista^{1,2}, E. Costa¹, I. Donnarumma¹, I. Lapshov¹, F. Lazzarotto¹,
L. Pacciani¹, M. Rapisarda³, P. Soffitta¹, A. Argan¹, G. Barbiellini^{4,5}, F. Boffelli⁶, A. Bulgarelli⁷,
P. Caraveo⁸, P.W. Cattaneo⁶, A. Chen⁸, F. D’Ammando^{1,10}, G. Di Cocco⁷, F. Fuschino⁷, M. Galli⁹,
F. Gianotti⁷, A. Giuliani⁸, C. Labanti⁷, P. Lipari², F. Longo^{4,5}, M. Marisaldi⁷, S. Mereghetti⁸, E. Moretti^{4,5},
A. Morselli¹⁰, A. Pellizzoni¹¹, F. Perotti⁸, G. Piano^{1,10}, P. Picozza¹⁰, M. Pilia^{11,12}, M. Prest¹², G. Pucella³,
A. Rappoldi⁶, S. Sabatini^{1,10}, E. Striani¹, M. Tavani^{1,10}, M. Trifoglio⁷, A. Trois¹, E. Vallazza⁴,
S. Vercellone¹³, V. Vittorini¹, A. Zambra¹⁴, L. A. Antonelli^{15,16}, S. Cutini^{15,17}, C. Pittori^{15,17}, B. Preger^{15,17},
P. Santolamazza^{15,17}, F. Verrecchia^{15,17}, P. Giommi^{15,18}, L. Salotti¹⁸

¹ INAF IASF Roma, Via Fosso del Cavaliere 100, I-00133 Roma, Italy
e-mail: ettore.delmonte@iasf-roma.inaf.it

² Dip. di Fisica, Università degli Studi di Roma “La Sapienza”, P.le A. Moro 5, I-00185 Roma, Italy

³ ENEA, Via E. Fermi 45, I-00044 Frascati (Rm), Italy

⁴ INFN Trieste, Padriciano 99, I-34012 Trieste, Italy

⁵ Dip. di Fisica, Università di Trieste, Via Valerio 2, I-34127 Trieste, Italy

⁶ INFN Pavia, Via Bassi, 6 I-27100 Pavia, Italy

⁷ INAF IASF Bologna, Via Gobetti 101, I-40129 Bologna, Italy

⁸ INAF IASF Milano, Via E. Bassini 15, I-20133 Milano, Italy

⁹ ENEA C.R. “E. Clementel”, Via Martiri di Monte Sole 4, I-40129 Bologna, Italy

¹⁰ Dip. di Fisica, Università degli Studi di Roma “Tor Vergata”, Via della Ricerca Scientifica 1, I-00133 Roma, Italy

¹¹ INAF Osservatorio Astronomico di Cagliari, loc. Poggio dei Pini, strada 54, I-09012, Capoterra (Ca), Italy

¹² Dip. di Fisica e Matematica, Università dell’Insubria, Via Valleggio 11, I-20100 Como, Italy

¹³ INAF IASF Palermo, Via U. La Malfa 153, I-90146 Palermo, Italy

¹⁴ Consorzio Interuniversitario per la Fisica Spaziale, Viale Settimio Severo 63, I-10133 Torino, Italy

¹⁵ ASI Science Data Center, Via G. Galilei, I-00044 Frascati (Rm), Italy

¹⁶ INAF Osservatorio Astronomico di Roma, Via di Frascati 33, I-00040 Monte Porzio Catone (Rm), Italy

¹⁷ INAF staff resident at ASI Science Data Center

¹⁸ Agenzia Spaziale Italiana, Unità Osservazione dell’Universo, Viale Liegi 26, 00198 Roma, Italy

Preprint online version: November 3, 2018

ABSTRACT

Context. Cygnus X-1 (Cyg X-1) is a high mass X-ray binary system, known to be a black hole candidate and one of the brightest sources in the X-ray sky, which shows both variability on all timescales and frequent flares. The source spends most of the time in a hard spectral state, dominated by a power-law emission, with occasional transitions to the soft and intermediate states, where a strong blackbody component emerges.

Aims. We present the observation of Cyg X-1 in a hard spectral state performed during the AGILE science verification phase and observing cycle 1 in hard X-rays (with SuperAGILE) and gamma rays (with the gamma ray imaging detector) and lasting for about 160 days with a live time of ~ 6 Ms.

Methods. We investigated the variability of Cyg X-1 in hard X-rays on different timescales, from ~ 300 s up to one day, and we applied different tools of timing analysis, such as the autocorrelation function, the first-order structure function, and the Lomb-Scargle periodogram, to our data (from SuperAGILE) and to the simultaneous data in soft X-rays (from RXTE/ASM). We concluded our investigation with a search for emission in the energy range above 100 MeV with the maximum likelihood technique.

Results. In the hard X-ray band, the flux of Cyg X-1 shows its typical erratic fluctuations on all timescales with variations of about a factor of two that do not significantly affect the shape of the energy spectrum. From the first-order structure function, we find that the X-ray emission of Cyg X-1 is characterized by *antipersistence* (anticorrelation in the time series, with an increase in the emission likely followed by a decrease), indicative of a negative feedback mechanism at work. In the gamma ray data a statistically significant point-like source at the position of Cyg X-1 is not found, and the upper limit on the flux is 5×10^{-8} ph cm⁻² s⁻¹ over the whole observation (160 days). Finally we compared our upper limit in gamma rays with the expectation of various models of the Cyg X-1 emission, both of hadronic and leptonic origin, in the GeV – TeV band.

Conclusions. The time history of Cyg X-1 in the hard X-ray band over 13 months (not continuous) is shown. Different analysis tools do not provide fully converging results of the characteristic timescales in the system, suggesting that the timescales found in the structure function are not intrinsic to the physics of the source. While Cyg X-1 is not detected in gamma rays, our upper limit is a factor of two lower than the EGRET one and is compatible with the extrapolation of the flux measured by COMPTEL in the same spectral state.

Key words. stars: individual: Cyg X-1 - gamma rays: observations - X-rays: binaries - X-rays: general

1. Introduction

Cygnus X-1 (Cyg X-1) is one of the brightest X-ray sources in the sky. It is a binary system composed of a compact object and the O9.7 Iab supergiant star HDE 226868, filling 97 % of its Roche Lobe, with a mass ranging between ~ 15 and $\sim 30 M_{\odot}$ (see for example Gierliński et al. 1999; Caballero-Nieves et al. 2009). The measurement of the mass of the compact object, with a range between $4.8 M_{\odot}$ and $14.7 M_{\odot}$ by Herrero et al. (1995) and $8.7 \pm 0.8 M_{\odot}$ from Shaposhnikov & Titarchuk (2007), suggests identification with a black hole. The distance to the binary system is measured as 2.1 ± 0.1 kpc by Ziolkowski (2005).

A characteristic feature of the black hole binaries (as Cyg X-1) in the X-ray band, discussed for example by Frontera et al. (2001) between 0.5 and 200 keV, is the existence of two well distinct emission states: “low/hard” and “high/soft”. The typical energy spectrum in the low/hard state, in which the source spends most of its time, is described well by a power-law ($E^{-\Gamma}$) with photon index $\Gamma \sim 1.7$ and a high-energy cutoff at ~ 150 keV. Instead, in the high/soft state the source is characterized by a strong blackbody component with $kT \sim 0.5$ keV and a soft power-law tail with Γ usually ranging between 2 and 3. An “intermediate” spectral state also exists, discovered by Belloni et al. (1996) in observations with the Proportional Counter Array (PCA) aboard the *Rossi X-Ray Timing Explorer* (RXTE), in which the flux is higher of about a factor of two with respect to the low/hard state and the spectrum is softer (with a photon index of ~ 2.1 and a blackbody component of ~ 0.36 keV temperature).

It is useful to note that the definition of low/hard and high/soft states derives from the observations at soft X-rays. When observing in hard X-rays, the condition reverses: the source is a factor of ~ 2 brighter in the low/hard state than in the high/soft one. The typical flux in the low/hard state is $\sim 8 \times 10^{-9}$ erg cm $^{-2}$ s $^{-1}$ in 20 – 40 keV and $\sim 3 \times 10^{-8}$ erg cm $^{-2}$ s $^{-1}$ in 1 – 10 keV. Although these definitions may be misleading when applied to the observations in hard X-rays reported in this paper, throughout the text we use the classification low/hard versus high/soft to comply with the classical literature on this source.

Cyg X-1 is a highly variable source in X-rays. Its variability is observed on any timescale, from months to seconds (see e. g. Brocksopp et al. 1999; Pottschmidt et al. 2003; Ling et al. 1997). In particular, in the hard X-ray range the experiments of the *Interplanetary Network* detected seven episodes of giant flaring in the 15 – 300 keV energy range, with a duration of 0.9 to 28 ks, peak flux of order of 10^{-7} erg cm $^{-2}$ s $^{-1}$ and fluence ranging from 5×10^{-5} erg cm $^{-2}$ to 8×10^{-4} erg cm $^{-2}$ (see Golenetskii et al. 2003). These outbursts were detected during both low/hard and high/soft spectral states, and, in general, the giant bursting events seem to maintain the spectral parameters (and likely the emission mechanisms) of the underlying state.

Recently, Cyg X-1 has been observed by Albert et al. (2007) above 150 GeV energy with the *Major Atmospheric Gamma Imaging Cherenkov* (MAGIC) telescope. A TeV excess of 4.1σ compatible with a point-like source and spatially consistent with Cyg X-1 was observed simultaneously with a hard X-ray flare taking place in the low/hard state

(~ 1.5 Crab - 1.2×10^{-8} erg cm $^{-2}$ s $^{-1}$ - in 20 – 40 keV with INTEGRAL (Malzac et al. 2008) and ~ 1.8 Crab in 15 – 50 keV of Swift/BAT and ~ 0.6 Crab in 2 – 12 keV of RXTE/ASM). The TeV excess was detected at the rising edge of the hard X-ray peak, one day before its maximum, while no variation is found in the soft X-ray emission. The source does not show any steady emission in the TeV band and the upper limits above ~ 150 GeV energy at the 95 % confidence level reach 2 % of the Crab Nebula flux.

Although Cyg X-1 is a well-known source in X-rays, very little information is known about its emission in gamma rays. During the first three cycles of observation (1991 – 1994) of the *Compton Gamma Ray Observatory* (CGRO), the source, in hard state, was detected by COMPTEL only between 2 and 5 MeV (see McConnell et al. 2000, for details). EGRET did not detect the source during that observation and the upper limit to the flux is of the order of 10×10^{-8} ph cm $^{-2}$ s $^{-1}$, posing no need for a high-energy cut-off. In the soft state, the spectrum of Cyg X-1 can be modelled with a power-law that extends with the same photon index ($\sim 2.5 - 3$) beyond 1 MeV and up to about 10 MeV as detected by COMPTEL (McConnell et al. 2002). Unfortunately in this case, no EGRET measurement is available.

In steady conditions, the radio emission of Cyg X-1 is stable during low/hard states (see Gleissner et al. 2004), except for rarely observed flares (Fender et al. 2006), and appears to be quenched below a detectable level during the high/soft state (Brocksopp et al. 1999). A non-thermal radio jet, extending up to $\sim 15 \times 10^{-3}$ arcsec with an opening angle less than 2° , was detected in VLBA observations by Stirling et al. (2001).

The X-ray flares and a radio-emitting jet allow the classification of Cyg X-1 as a microquasar, as described by Mirabel & Rodríguez (1999). The high-energy particles in the radio-emitting jet are likely to produce gamma rays as well (see Dubus 2007). Following the model by Zdziarski & Gierliński (2004), another possible source of gamma rays, especially in the low/hard spectral state, is the high-energy tail of the electron distribution in the corona. Instead in the high/soft state, the energy spectrum does not show an energy cutoff, as confirmed by the COMPTEL detection up to ~ 10 MeV (McConnell et al. 2002) and a gamma ray emission above this energy is expected.

AGILE (Tavani et al. 2008) is the first satellite mission sensitive to gamma rays (in 30 MeV – 30 GeV) flown after EGRET. It observed Cyg X-1 for ~ 160 days in four different pointings during its first observing cycle. Thanks to the X-ray monitor SuperAGILE (Feroci et al. 2007), the source is observed at the same time in the hard X-ray band (between 20 and 50 keV). AGILE can continuously monitor the source, with a duty cycle of about 50 %. Other scanning instruments, such as RXTE/ASM or Swift/BAT, observe each source many times a day but for a shorter duration, and the duty cycle is usually shorter than 10 %.

In this paper we report the probably longest uninterrupted observation of Cyg X-1 in the hard X-ray and gamma ray bands from the AGILE data, complemented and extended at lower energy (2 – 12 keV) with the information from the public web archive^{1 2} of the All Sky Monitor (ASM) aboard RXTE. After the summary of the

¹ http://heasarc.nasa.gov/xte_weather/

² http://xte.mit.edu/ASM_lc.html

observations (given in Sect. 2) and the description of the methods of analysis (Sect. 3), we report the results of the data analysis in X-rays (Sect. 4) and gamma rays (Sect. 5). Finally, in Sect. 6 we discuss our findings and draw our conclusions in Sect. 7.

2. Observations

AGILE observed the Cygnus region four times during the first cycle of observations: from early November until mid December 2007 (44 days, hereafter observing block 1 or OB1), in the second and third decades of April 2008 (20 days, hereafter observing block 2 or OB2), in the second half of May and whole June 2008 (51 days, hereafter observing block 3 or OB3), and from mid October until the beginning of December 2008 (45 days, hereafter observing block 4 or OB4). The first observing block began during the satellite science verification phase, which lasted from July until November 2007.

Each observation in the AGILE pointing plan usually lasts from 2 to 4 weeks to favour the photon collection in the gamma ray band. The main constraint in the AGILE pointing strategy is the angle between the Sun and the solar panels, which has to be fixed at $90^\circ \pm 1^\circ$. Because of this solar constraint, the pointing of AGILE, hence the position of the sources in the field of view, drifts by $\sim 1^\circ$ per day. For this reason the off-axis angle (the distance between the source position and the satellite boresight) is not constant during the observation. The value of the off-axis angle of Cyg X-1 during the four observing blocks ranges from 2.4° to 32.7° . The exposure of each observing block, as reported in the table, is computed as the total time in which the source is observed, excluding the duration of the satellite passages through the South Atlantic Anomaly (SAA) and the source occultation by the Earth. Following these criteria, the total on-source exposure amounts to 6.1×10^6 s. We show in table 1 the details (start and end date, off-axis angle and exposure) of the observing periods in the AGILE observation.

3. Data reduction and analysis

3.1. X-rays

SuperAGILE (see Feroci et al. 2007, for a description) is a coded aperture instrument, and its data analysis software is highly customized, as frequently happens for similar experiments. The data of SuperAGILE are processed using the Enhanced Multi sky Imaging (EMI) software package, suitable for decoding the images of bright sources in moderately crowded fields (see Feroci et al. 2010, for details). In the observation reported in this paper, Cyg X-1 is always the brightest source in the field of view, making EMI a reliable method of data processing.

SuperAGILE is a 1-D imager with a field of view composed of two orthogonal and overlapping regions, of $107^\circ \times 68^\circ$ each at zero response. In the central area, of $68^\circ \times 68^\circ$, both coordinates are encoded, thus giving twice a 1-D imaging, and the sensitivity on axis is of the order of 15 mCrab at 5σ in one day with an energy resolution of ~ 8 keV FWHM. During all the observations, Cyg X-1 is in the twice 1-D region, with an off-axis angle ranging from 2.4° to 32.7° (see table 1). As studied in the SuperAGILE ground and in-flight calibrations (Evangelista et al. 2006;

Feroci et al. 2008), the variation of the instrument Point Spread Function in this range of off-axis angles does not affect significantly the imaging response.

The output of the EMI software, for all the sources detected in an image above a significance level of 5σ , is the count rate normalized with the instrument effective area convolved with a Crab-like spectrum, making it independent of the source position in the field of view. Throughout this paper we refer to the normalized counting rate defined above, and as a reference, the value for the Crab Nebula is $0.15 \text{ cts cm}^{-2} \text{ s}^{-1}$. The normalized rates from EMI have been calibrated by means of a raster scan of pointings toward the Crab Nebula during the AGILE science verification phase and also verified with other bright sources using the Swift/BAT transient monitor results³. The uncertainty on the normalized rate values quoted throughout this paper includes both the statistical and systematic components (see Feroci et al. 2010, for details). Since the systematic uncertainty applies to the absolute value of the flux but not to relative values of subsequent measurements in the same pointing, in the plots we show only data points with statistical errors, separately showing the systematic uncertainty on the flux calibration.

We accumulated the “correlated” energy spectrum of Cyg X-1, which is the flux of the source extracted from images integrated in different energy intervals. The spectrum of Cyg X-1 was extracted in bins of 2 keV amplitude, from 20 to 50 keV, by using the EMI software. Since the source is bright, the significance of the source in the images is greater than 5σ in all the energy intervals. The spectrum is accumulated separately in the two 1-D directions and then fitted simultaneously using the software package XSPEC v. 12.3.0 (Dorman et al. 2003).

3.2. Gamma rays

We completed the study of Cyg X-1 with the observation by the AGILE gamma ray imaging detector (GRID), sensitive in the energy band between 30 MeV and 30 GeV. The data are analysed with the AGILE Standard Analysis Pipeline (see e. g. Vercellone et al. 2008, for a detailed description). We accumulated the count map, calculated the exposure map, and estimated the map of the gamma rays from the Galactic Background only above 100 MeV and for events flagged as confirmed gamma rays (`filtercode=5`) after excluding the data collected inside the SAA (`phasecode=18`). The region of interest in the study of Cyg X-1 reported in this paper has a 40° radius, inside a map of 80° radius with 0.5° bin size. We used a particular application of the AGILE maximum likelihood (ALIKE) procedure, called `ALIKESingle`, to search for the detection of sources at a specified position. Every run of the `ALIKESingle` software provides the user with the significance of the maximum likelihood technique applied at the input position and either the flux or the 2σ upper limit in case a point-like source is detected or not, respectively. To sum all the data of the whole gamma ray observation, all the maps are centred on the same galactic coordinates ($l = 88.0^\circ$, $b = -12.0^\circ$).

³ <http://swift.gsfc.nasa.gov/docs/swift/results/transients/>

4. Results in the X-ray band

4.1. The hard X-ray variability

Thanks to the continuous monitoring of SuperAGILE, a measure of the variability of Cyg X-1 with the resolution of about 3 ks from the standard EMI pipeline is obtained. We adopted this resolution, corresponding to an AGILE orbit, to guarantee the statistical significance of the source detection in each time bin and to favour the joint analysis with RXTE/ASM, although the SuperAGILE data allow for finer time resolution. A synthetic view of the normalized counting rate measured by SuperAGILE is given in Fig. 1, together with the measure of RXTE/ASM in the same time interval. The time bin of ~ 3 ks is used for both instruments. As a reference, the counting rate of the Crab Nebula is $0.15 \text{ cts cm}^{-2} \text{ s}^{-1}$ in SuperAGILE and 75 cts s^{-1} in RXTE/ASM.

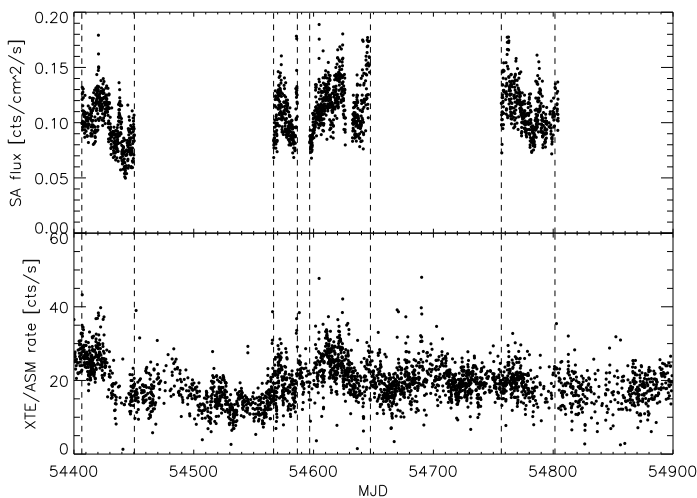


Fig. 1. Superposition of the SuperAGILE (upper panel) and RXTE/ASM (lower panel) fluxes of Cyg X-1 during the observation. The error bars are omitted for clarity and the RXTE/ASM data are rebinned with 3 ks time bin. The vertical dashed lines limit the observing blocks. The normalized rate of the Crab Nebula is $0.15 \text{ cts cm}^{-2} \text{ s}^{-1}$ in SuperAGILE and 75 cts s^{-1} in RXTE/ASM.

The continuous and uninterrupted source covering of SuperAGILE allows us to detect possible flaring episodes and also to study the flux with higher time resolution, if compared for example to Swift/BAT with its higher sensitivity in a similar energy band (15 – 50 keV) but a completely different pointing strategy with shorter “snapshots” at higher sensitivity but lower duty cycle.

By comparing the rate of Cyg X-1 measured by RXTE/ASM during our observation with typical values in the hard spectral state ($20 - 30 \text{ cts s}^{-1}$) and in the transitions to the soft spectral state (more than $80 - 100 \text{ cts s}^{-1}$ on June 1996 (Frontera et al. 2001) or September 2001 (Pottschmidt et al. 2003)), we derive that the source did not reach the soft state during our observation. We study with more completeness the spectral state during the AGILE observation by means of a colour-colour diagram from the public data of RXTE/ASM, plotted in Fig. 2. In the figure the whole dataset of RXTE/ASM (with daily

integration between MJD 50087 and 54801) is represented by grey dots and we superimpose the data simultaneous to the AGILE observation (black dots), the points (squares) during the soft state between MJD 50230 and 50307 (see Zdziarski et al. 2002) and during the intermediate state of MJD 52797 – 52801 (crosses), reported by Malzac et al. (2006). From the distribution of the black points in the colour-colour diagram, it is possible to see that Cyg X-1 remained in the low/hard spectral state for the whole duration of the AGILE observation.

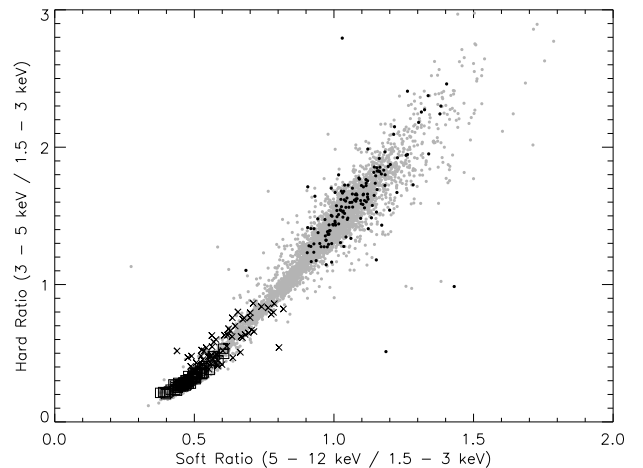


Fig. 2. Colour-colour diagram of Cyg X-1 from the public data of RXTE/ASM with the hard ratio (estimated from the counting rate in 5 – 12 keV divided by the one in 1.5 – 3 keV) as a function of the soft ratio (from the fraction between the rate in 3 – 5 keV and the one in 1.5 – 3 keV), similarly to Reig et al. (2002). The grey dots are the daily average of the whole dataset (from MJD 50087 until 54801), the black dots are the daily average of the data simultaneous to the AGILE observation, the black squares are the data in the soft state from MJD 50230 until 50307 (see Zdziarski et al. 2002) and finally the black crosses are the dwell averages in the intermediate state from MJD 52797 until 52801 (see Malzac et al. 2006) since this state lasted for only five days.

We select two different timescales to estimate the source counting rate in the SuperAGILE band: one satellite orbit, with net exposure of ~ 3 ks, and one day, with exposure of ~ 40 ks. The normalized rate of Cyg X-1 on orbital timescale is plotted in Fig. 3. All the plots have the same vertical scale to compare the source variability. The rate is converted into units of $\text{erg cm}^{-2} \text{ s}^{-1}$ using a conversion factor derived from the fit of the average energy spectrum.

In the plots the characteristic slow variations of the emission of Cyg X-1 are clearly detected, with a typical timescale of 30 – 50 days in which the source flux changes up to a factor of ~ 3 . Superimposed to this slow modulation, a faster and erratic variability, with timescale of about one day and a maximum flux variation of the order of two, can be seen. In the same figures it is also possible to appreciate the short time flickering of Cyg X-1, on the scale of a few hours. Although some periods of rapid flux increase

were detected, for example around MJD 54420, 54605 or 54648, large flares were not detected during the AGILE observation.

SuperAGILE always stores and transmits all the detected counts (photon-by-photon operative mode). We could then measure the normalized rate of Cyg X-1 accumulating images with a time bin of ~ 300 s exposure, a trade-off between time and statistical quality of the images. We excluded the time intervals corresponding to the SAA and to Earth occultation. Usually we cut the SuperAGILE data with an energy threshold fixed at 20 keV to avoid the systematics due to the variation of the instrument temperature. Instead, in the integration time of ~ 300 s the temperature, and consequently threshold, variation is small, thus we can lower the energy threshold down to 17 keV. We show for example in Fig. 4 the lightcurve of Cyg X-1 with a resolution of ~ 300 s between MJD 54604 and 54605, during a flaring episode. The higher time resolution allows the short-time variability superimposed to the main flux variation to be appreciated.

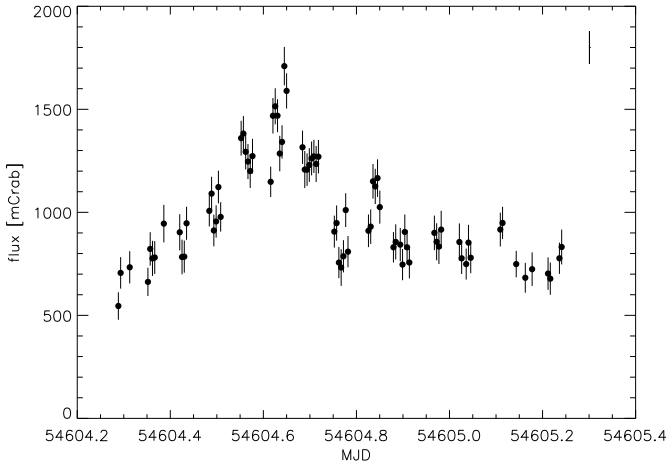


Fig. 4. SuperAGILE lightcurve of the source flux increase between MJD 54604 and 54605 in the energy interval 17 – 50 keV with a bin size of ~ 300 s. The gaps in the lightcurve are due to the passage of the satellite through the SAA and to the source occultation by the Earth. Only the statistical uncertainty is shown on the points in the plots. The average systematic uncertainty on the flux calibration is plotted in the top right angle.

The availability of the photon-by-photon data also permits building of the energy spectra. To check for spectral variability possibly associated with the observed flux variations, we studied the energy spectrum of Cyg X-1 in three flux states: average (from MJD 54610 until 54612), faint (between MJD 54597 and 54599), and bright (MJD from 54761 to 54762). A simple power-law, the model `pegpwlw` of XSPEC v.12.3.0 (Dorman et al. 2003), provides a good fit to the spectrum in the 20 – 50 keV energy band (see Fig. 5). The results of the spectral fit are summarized in Table 2. The spectral shape of the source does not show significant variations despite a flux variation of nearly a factor of two, except for a marginal indication of a small softening at lower flux.

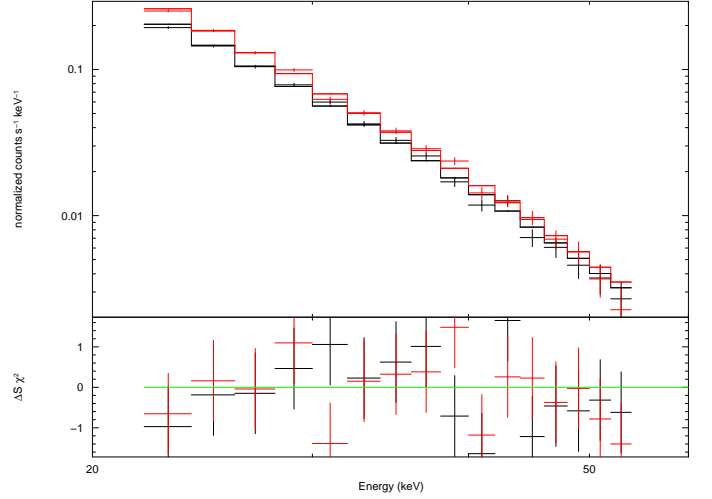


Fig. 5. Spectrum of Cyg X-1 from the SuperAGILE images in the X direction showing the bright (MJD 54761 – 54762, 75 ks exposure, $0.17 \text{ cts cm}^{-2} \text{ s}^{-1}$, red in colour version) and faint (MJD 54597 – 54599, 92 ks exposure, $0.08 \text{ cts cm}^{-2} \text{ s}^{-1}$, black in colour version) flux states of the source. The parameters of the fit for the images in both directions are reported in Table 2, where the uncertainties are at a 90 % confidence level and include a 5 % systematic error.

4.2. Correlation between soft and hard X-rays

We studied the source variability in the SuperAGILE data with the sampling time of one day, by accumulating the images separately in two energy bands, low energy (LE) from 20 to 25 keV and high-energy (HE) from 25 to 50 keV, with a net exposure of ~ 40 ks for each image. A hardness ratio is computed as the rate in HE divided by the one in LE. The plots of the normalized rate and hardness ratio are shown in Fig. 6. We find that, during the observing blocks 1, 2 and 4, the hardness ratio is roughly constant despite rate variations by roughly a factor of ~ 2 , with a few exceptions; for example, between MJD 54441 and 54443, the hardness ratio increases in coincidence with an enhancement of the counting rate after a local minimum, owing to a flux reduction of about 50 % on MJD 54442. In the observing period 3, the hardness ratio shows a general linear increase, with short-term fluctuations superimposed, corresponding to a similar trend in the rate. The comparison with the data in 2 – 12 keV (see Fig. 1) shows that the soft X-ray flux decreases at the same time thus confirming the higher hardness.

We investigated the contribution of the emission mechanism at different energy ranges by studying the correlation between the soft (from the RXTE/ASM public archive) and hard (SuperAGILE observation) X-ray bands. We removed the dips simultaneous to the inferior conjunction of the binary system (observed by Mason et al. 1974; Holt et al. 1979; Friedhorsky et al. 1995), with the stellar companion passing between the black hole and the observer along the line of sight, using the orbital solutions for HDE 226868 reported by Lasala et al. (1998), with a period of 5.5998 days. We then rebinned the lightcurves of both instruments on a common timescale with the same bin size of six hours, in order to increase the statistic of the measurement and improve the chance of having at least one ASM measurement

in the bin. From the superposition of the lightcurves and the hardness ratio for each observing block, shown in Fig. 7, we can see that there are intervals of time of increased fluctuation in the hardness ratio. For example in the OB1, the hardness ratio is almost constant between MJD 54406 and 54427, and its variability increases until MJD 54442. Simultaneous to the increased variability, we can see that the hard X-ray flux shows a flaring episode of about five days duration reaching ~ 800 mCrab around MJD 54438, while the soft X-ray flux has a decreasing trend. A similar behaviour is shown in the OB4, with an increase in the hardness ratio between MJD 54785 and 54793, corresponding to a bump in hard X-rays, peaking around 500 mCrab on MJD 54788, while the soft X-ray emission is almost constant at ~ 250 mCrab level. At the end of the OB3, the flux measured by SuperAGILE increases up to ~ 1500 mCrab while the measure by RXTE/ASM remains between 200 and 400 mCrab, but in this period the source is at an off-axis angle of about 32° , where the flux estimation is less accurate. Unfortunately, the RXTE/ASM data are sparse in these time intervals and consequently we cannot draw any serious conclusion. To verify if we can find any variation in the source photon index, we extracted the energy spectra of these episodes, but we did not find any significant differences from the ordinary values. For example, the photon index of the power-law that fits the spectrum accumulated in the OB4 between MJD 54787 and 54789 is consistent with the values reported in Table 2.

To investigate possible correlations between the source emission in soft and hard X-rays, we show in Fig. 8 the scatter plot of the fluxes of SuperAGILE and RXTE/ASM, each one converted into Crab units for clarity. A certain degree of correlation appears in the plot, although the value of the correlation coefficient is 0.03 and does not allow establishment of a formally significant correlation, even with more than 600 degrees of freedom. In the lower lefthand region of the plot (between ~ 150 and ~ 250 mCrab values for the ASM rate), we can see the data corresponding to the intervals in which the source emission is increased in the hard X-ray range and is almost constant in soft X-rays. We also computed the cross-correlation of the RXTE/ASM and SuperAGILE lightcurves (both accumulated with six hours resolution), and we did not find any time lag greater than the bin size of six hours. The degree of correlation at zero time lag is higher in the OB1 (0.73) and OB2 (0.69) than in the OB3 (0.54) and OB4 (0.55).

4.3. Analysis of the structure function

The SuperAGILE data are not well-suited to timing analysis of Cyg X-1 using the standard tools, e.g. the fast fourier transform. In fact, the measured rate is a few counts per second, depending on the position of the source in the field of view, and the occultation of the source by the Earth produces a discontinuity (and consequently a windowing effect) on the time series.

As explained for example by Hughes et al. (1992), a useful tool for studying the time variability of a physical quantity with such sampling characteristics is the first-order structure function, simply referred to as “structure function” or SF. This function is commonly used in the analysis of time series (see e.g. Rutman 1978), has been introduced in astronomy by Simonetti et al. (1985) mainly for the study of active galactic nuclei, and is also insensitive to

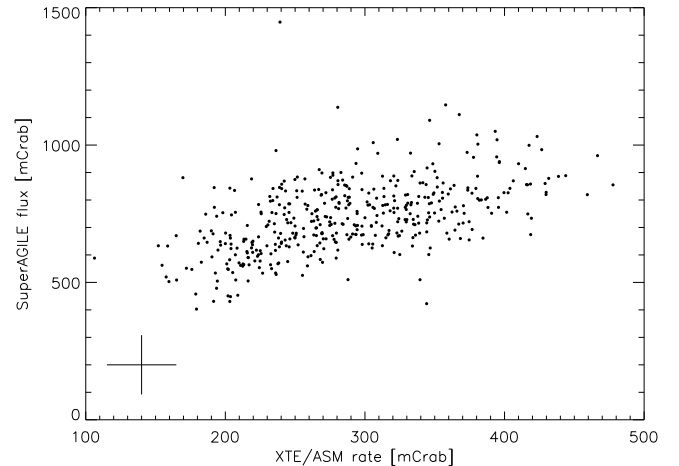


Fig. 8. Scatter plot of the SuperAGILE (20 – 50 keV) vs RXTE/ASM (2 – 12 keV) flux, both separately converted into Crab units and rebinned on a common timescale with a bin size of six hours. The typical uncertainty is plotted for clarity only in the lower left corner.

temporal gaps in the data. The insensitivity of the structure function to gaps in the data is extremely important for satellites in low earth orbit, such as AGILE, whose observations are interrupted by the occultation of the source by the Earth and by the passage of the satellite through the South Atlantic Anomaly.

The first-order SF is defined by Simonetti et al. (1985) as $D_f^1(\tau) \equiv \langle [f(t + \tau) - f(t)]^2 \rangle$ and in our case it can be estimated as

$$D_f^1(\tau) = \frac{1}{N(\tau)} \sum [f(t + \tau) - f(t)]^2 \quad (1)$$

where the brackets $\langle \rangle$ indicate the average, τ is the time lag, $f(t + \tau)$ and $f(t)$ represent the flux at time $t + \tau$ and t , respectively, and $N(\tau)$ is the number of pairs considered in the average.

A plateau at small time lags (often referred to as “horizontal branch”) is common of the SFs of the active galactic nuclei in optical (see for example Paltani et al. 1997) and gamma rays (see Nandikotkur et al. 1997) and is generally produced by the white noise (uncorrelated flux) of the source emission, yielding a constant value independent of the time lag. A monotonic region is found at increasing lags, where the SF approximately follows a power-law, $D_f^1(\tau) \propto \tau^{2H}$ (see for example Nandikotkur et al. 1997). The parameter H is also known as the Hurst exponent and is used in describing non-stationary processes. Systems with $0.5 < H < 1$ are *persistent*: an increasing trend in the past is probably followed by a similar increasing trend in the future. Conversely, if $0 < H < 0.5$ the process shows *antipersistence* and an increase in the past is probably followed by a decrease in the future. Finally, the minima in the structure function indicate typical timescales of the system (Nandikotkur et al. 1997).

We computed the structure function of the normalized rate of Cyg X-1, extracted separately in the four observing blocks and the two energy bands (20 – 50 keV of SuperAGILE and 2 – 12 keV of RXTE/ASM), estimating the rate with the time resolution of one orbit (~ 3 ks of

net exposure) for SuperAGILE and one dwell (~ 90 s) for RXTE/ASM. The SFs of the SuperAGILE data are shown in Fig. 9, from top (OB1) to bottom (OB4). Similarly, the structure function of RXTE/ASM data is shown in Fig. 10 with the same disposition of OB1 on top and OB4 at the bottom.

The first evident feature in the structure function in both energy bands is the absence of the “horizontal branch”, indicating that the variability of Cyg X-1 is correlated even at lags of the order of 10^4 s, the smallest timescale sampled in our observations. The time lag values in the data span more than two orders of magnitude, from $\sim 10^4$ s up to $\sim 4 \times 10^6$ s, with the OB2 the only exception, limited to $\sim 2 \times 10^6$ s, since this observing period is shorter than the others.

The structure functions in the hard X-ray band show a monotonic increase between time lags of about 10^4 up to $\sim 10^6$ s. Above $\sim 10^6$ s the curve is less smooth, many fluctuations appear and, in some cases, a few minima are found. Similar behaviour is qualitatively found in the soft X-ray band, and also in this case the monotonic region extends between $\sim 10^4$ s and $\sim 2 \times 10^6$ s. In the OB1 and OB2 the structure function in the two energy bands are comparable, while in the OB3 and OB4 the SuperAGILE data are different from the RXTE/ASM data, which show a flatter power-law, with less pronounced fluctuations.

We define the minima as these values for which the structure function is more than 3σ far from the smoothed value. With this method we find minima only in the OB2, at 1.42×10^6 s (corresponding to 16.5 days) in SuperAGILE and at 0.57×10^6 s (6.7 days), 1.15×10^6 s (13.3 days), and 1.53×10^6 s (17.7 days) in RXTE/ASM. Interestingly, these three minima are all multiples of the same Δt of 6.7 days, of which 13.3 days is the double and 17.7 days has a ratio of 4/3. The minimum in the SuperAGILE data has a ratio of 5/2 with the Δt of 6.7 days. We do not find minima in the other observing periods, only fluctuations near the time corresponding to half of the duration of the observation, where the scattering of the data increases. This is the case, for example, of the broad “valleys” in the SuperAGILE SFs of the OB3 (around gap of 4×10^6 s) and OB4 (about 3×10^6 s) or the wide fluctuation in the RXTE/ASM sample of the OB1 (between 2 and 3×10^6 s).

To confirm our results in hard X-rays, we repeated the analysis of the structure function using the publicly available Swift/BAT data, in an energy band similar to SuperAGILE (15 – 50 keV). Searching with the same significance level, we found minima at 0.42×10^6 s (4.9 days), 0.99×10^6 s (11.5 days), and 1.42×10^6 s (16.5 days) in the OB2. The last (1.42×10^6 s) is at the same position as the one found in the SuperAGILE data. The analysis of the Swift/BAT data corresponding to the OB1, OB3, and OB4 confirms the absence of minima in the SF.

To verify that the structure function is indeed insensitive to windowing and aliasing of the time series, (e. g. Hughes et al. 1992), we computed the SF of a simulated time series. At the same time values of the OB2, shown in Fig. 3, we simulated the flux by extracting with a random uniform distribution between the minimum and maximum measured values. Then, we computed the structure function of this simulated time series and applied the same algorithm used to find the position of the minima. After 10^4 simulations, our algorithm found a fake minimum only

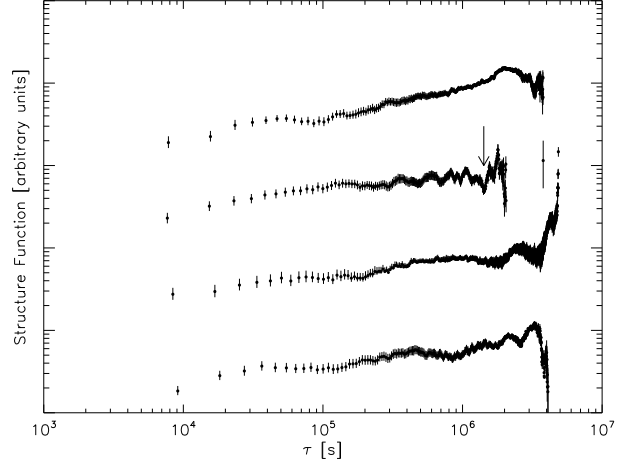


Fig. 9. Superposition of the first-order structure function of the SuperAGILE flux extracted from the orbital integration. From top OB1 to OB4 are shown. The arrow mark the position of the minimum

in 71 occurrences, which is the 0.7 %, thus confirming the goodness of our results.

Finally, we fitted the function $\log[D_f^1(\tau)]$, independently in the four observing blocks and the two energy bands, to estimate the Hurst exponent H . Only in two cases, OB3 in the SuperAGILE data and OB1 in the RXTE/ASM data, the structure function shows a break and it is not possible to apply the same fit to the complete curve, thus the interval has been split in two, fitted separately. In the other cases, the structure function is described by a single fit. The ranges of time lag in which the fits are applied and the resulting value of the H exponent are reported in Table 3 (SuperAGILE data) and Table 4 (RXTE/ASM data). In all the observing blocks and in both energy bands, H is always significantly lower than the critical value of 0.5, indicating *antipersistence* in the source emission.

4.4. Alternative methods of timing analysis

We adopted additional and alternative methods of timing analysis to verify the timescales of the system found in the structure function: Lomb-Scargle periodogram and autocorrelation function. These tools were chosen to comply with the structure of our time series, which is very unevenly spaced.

The Lomb-Scargle periodogram is an algorithm specifically developed to calculate the power spectrum of such non-uniformly spaced data (Lomb 1976; Scargle 1982; Horne & Baliunas 1986). This tool has been already adopted in the analysis of the long-term variability of Cyg X-1, for example by Rico (2008) and Benlloch et al. (2004), to search for the superorbital period. Only some of the timescales from the structure function are also present in the periodogram of the OB2: 6.7 and 13.3 days in the RXTE/ASM data and 4.9 and 16.5 days in the Swift/BAT data. Other timescales, in contrast, are not found in the Lomb-Scargle diagram, such as the 16.5 days in SuperAGILE, the 17.7 days in RXTE/ASM and the 11.5 days in Swift/BAT.

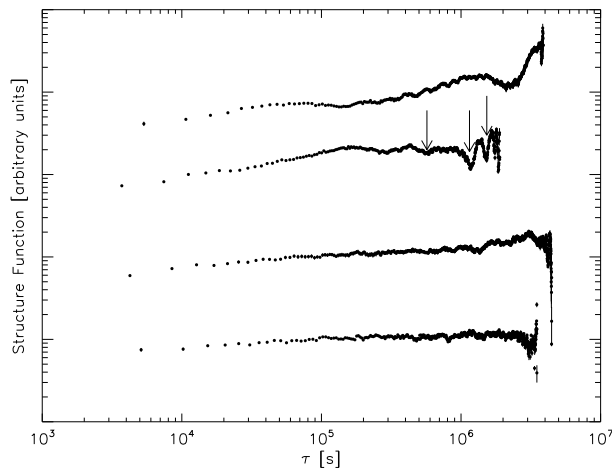


Fig. 10. Superposition of the first-order structure function of the RXTE/ASM flux extracted from the “dwell” of 90 s duration. From top OB1 to OB4 are shown. The uncertainty on the SF is generally smaller than the symbol used in the plot. The arrows mark the position of the minima.

By using the Lomb-Scargle periodogram, Rico (2008) finds a superorbital modulation in the flux of Cyg X-1 with a period of 326 ± 2 days. The SuperAGILE data span a total duration of ~ 395 days, but the observing periods are shorter and not evenly distributed during this time. For this reason we cannot significantly test the presence of such superorbital modulation, as confirmed by our attempts to fold our data on the periods mentioned above.

We calculated the autocorrelation function from the SuperAGILE and RXTE/ASM data in the four observing blocks (defined in Table 1) after removing the dips produced by the inferior conjunction of the binary system and after rebinning the data at six hours. Similar to Maccarone et al. (2000), we computed the autocorrelation function in three energy bands: 20 – 50 keV of SuperAGILE, 1.5 – 5 keV given by the sum of the A and B bands of RXTE/ASM and 5 – 12 keV from the ASM C band. Apart from the peak at zero lag, no other peak is found, indicating that the source emission does not show periodicity in all energy ranges. Some differences in the width of the autocorrelation are found depending on the energy band, but our analysis does not show any definite trend.

5. Results in the gamma ray energy band

We analysed the GRID data to search for emission of Cyg X-1 above 100 MeV using different timescales: one day, five days, a single observing block, and the complete AGILE observation. For the timescales of one and five days, we analysed all the contiguous time intervals included in the four observing blocks independently. Compared to the real time, the live time is typically ~ 40 ks and ~ 200 ks for the two types of integrations, respectively, owing to the Earth occultation and the satellite passages through the SAA. Cyg X-1 is not detected as a point-like source on any timescale and the 2σ upper limit depends on the duration of the observation: $\sim 100 \times 10^{-8}$ ph cm $^{-2}$ s $^{-1}$ in one day, and $\sim 50 \times 10^{-8}$ ph cm $^{-2}$ s $^{-1}$ and $\sim 30 \times 10^{-8}$ ph cm $^{-2}$ s $^{-1}$ in one observing block. The value of the upper limit also

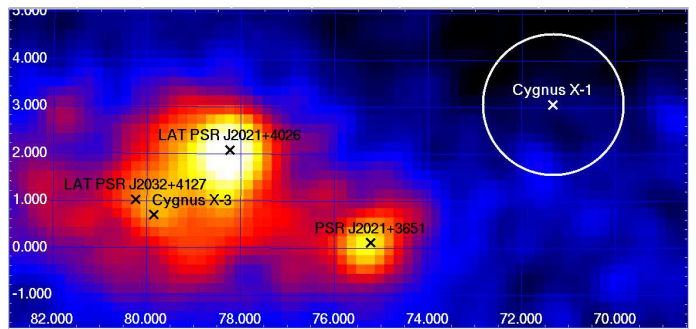


Fig. 11. Sum of the GRID count maps of the four observing periods. The data are smoothed with a Gaussian shape of 3 pixel standard deviation, and the circle at the position of Cyg X-1 has a radius of 1.5° , corresponding to the instrument point spread function at ~ 200 MeV.

depends on the position of the source within the GRID field of view (see Table 1), which influences the effective area, particularly in the last part of the OB1, where the upper limits are $\sim 30\%$ higher.

To find our deepest upper limit on the source flux, we accumulated the maps of the whole observation, as shown in Fig. 11. The circle at the position of Cyg X-1 has a radius of 1.5° , corresponding to the GRID point spread function at ~ 200 MeV. The source is not detected and the upper limit above 100 MeV is $\sim 5 \times 10^{-8}$ ph cm $^{-2}$ s $^{-1}$. From the gamma ray map, it is possible to see that the closest source is PSR J2021+3651, located at a distance of 4.6° from Cyg X-1, well outside the point spread function. We can then exclude the contamination by field sources.

6. Discussion

The AGILE mission observed Cyg X-1 ~ 4 month-long continuous periods of time during the science verification phase and the observing cycle 1, between July 2007 and December 2008, for a total net exposure to the source of about 6 Ms. Because of the AGILE pointed strategy, during these observing periods the monitoring of the source is continuous, interrupted only by the periodic occultation by the Earth. Under this condition, the SuperAGILE data on Cyg X-1 are a unique set in the hard X-rays. Other hard X-ray experiments provided monitoring data on Cyg X-1, but all of them are either (i) sparse, short snapshots of the source, e.g. CGRO/BATSE (Crary et al. 1996; Ling et al. 1997; Brocksopp et al. 1999; Zdziarski et al. 2002) and Swift/BAT (Rico 2008) or (ii) short pointed observations (e.g., INTEGRAL/ISGRI: Cadolle Bel et al. 2006). By taking as a reference a colour-colour diagram built with the data of the RXTE/ASM in the soft X-ray energy range, we verified that Cyg X-1 remained in its low-hard state the whole time.

6.1. X-ray variability on short timescales

We used the SuperAGILE data to systematically investigate the source variability over our 160 days of monitoring on different timescales, from ~ 300 s to the ~ 1 -hour timescale, up to week-long time segments. For the time periods when the source exhibited a significant variability on the minute timescale, we also (un-

successfully) searched for potential flares on the tens-of-second to subsecond-timescale in the SuperAGILE raw lightcurves. Such variability has been observed in the past by Gierliński & Zdziarski (2003) on the ms timescale in the soft X-rays with RXTE/PCA, and by Golenetskii et al. (2003) on the hour timescale in the hard-X/gamma rays using the experiments of the InterPlanetary Network. Both types of variability were observed with the source in both soft and hard spectral states in a flux range of a $\text{few} \times 10^{-7} \text{ erg cm}^{-2} \text{ s}^{-1}$ (corresponding to a luminosity of $\sim 10^{38} \text{ erg s}^{-1}$, assuming a distance of 2 kpc) in the energy ranges 3 – 30 keV and 15 – 300 keV, respectively. During our observations we detected several flares on timescales of a few hours to half a day, at times corresponding to MJD 54420.4, 54585.6, 54604.6, 54607.9 and 54646.5. Contrary to the cases cited above, which involved flux variability of one order of magnitude, these flares correspond to flux increases of approximately a factor of 2 – 3, passing from $\sim 5 - 6 \times 10^{-9} \text{ erg cm}^{-2} \text{ s}^{-1}$ to maxima of about $\sim 1.4 \times 10^{-8} \text{ erg cm}^{-2} \text{ s}^{-1}$, as measured on the hour timescale in the 20 – 50 keV energy range. Results similar to ours were also reported by Brocksopp et al. (1999) in a study based on data of BATSE and RXTE/ASM, and by Malzac et al. (2008) using INTEGRAL/ISGRI (in the energy band 18 – 40 keV). In particular, the 18 May 2008 (MJD 54604) flaring episode reported by Neronov et al. (2008), with a duration of about 8 hours, is among the flares observed by SuperAGILE during the OB3. The flux measured by SuperAGILE in 20 – 50 keV between 15:02 and 15:36 UT, when INTEGRAL/ISGRI detected the maximum of the source emission, is ~ 1.5 Crab.

6.2. Long-term variability

Interestingly, with the exception of the flares discussed in the previous section, during the SuperAGILE monitoring the hard X-ray flux of Cyg X-1 remained quite stable around $\sim 5 - 6 \times 10^{-9} \text{ erg cm}^{-2} \text{ s}^{-1}$, with fluctuations on much longer timescales. We investigated this long-term variability by using different analysis tools. The SuperAGILE data are characterized by long gaps between the observing periods, and shorter gaps due to the Earth's occultation in every orbit. For this reason we applied the analysis of the structure function for the first time in the study of a Galactic binary source, but frequently used for the active galactic nuclei in the radio and gamma ray energy bands (see for example Hughes et al. 1992; Simonetti et al. 1985; Nandikotkur et al. 1997). We performed a comparative analysis in the hard and soft X-rays, complementing the SuperAGILE data with those of RXTE/ASM available in the public archive. Since the slope of the structure function is connected to the probability of long duration trends in the emission mechanism, while the minima in the same function are related to the typical timescales of the same process, we address the two topics separately.

By using a logarithmic fit to the structure function versus the time lag, we find that, throughout the whole period of our analysis, the Hurst exponent H is significantly below the critical value of 0.5, indicating that the source is *antipersistent*. This *antipersistence* is a property of random non-stationary processes and indicates that an increase in the past is likely to be followed by a decrease in the future (Kärner 2005). *Antipersistent* systems are not common in nature and show a dominant negative feedback at

work that produces “oscillations”, i. e. repetition of similar features but without periodicity, because the distance in time is not constant (see for example Koutsoyiannis 2008). Gil-Alana (2006) and Kärner (2005), for example, find *antipersistence* in the climatological study of the time series of the temperature in various layers of the Earth atmosphere and discuss possible mechanisms of negative feedback (ice albedo, water vapour and clouds). On the other hand, Alvarez-Ramirez et al. (2002), always by means of the Hurst exponent, find that the crude oil market is a *persistent* process with long-run memory effects and different timescales at work: the “oscillations” from days to weeks are apparently generated by the action of market speculators and are superimposed on a long-time trend, with characteristic timescale of weeks to three months.

The description of the *antipersistent* systems matches the behaviour of Cyg X-1, whose luminosity does not seem to vary on long timescales and shows non-periodic “oscillations” around an average value of $\sim 2 \times 10^{37} \text{ erg s}^{-1}$. This aperiodic variation is well known especially in the low/hard spectral states, (see for example Makishima et al. 2008, and references therein). A complete discussion of the possible negative feedback mechanisms in the emission of Cyg X-1 would require a detailed analysis of the interactions between the various components at work (stellar wind, accretion disk, Comptonizing plasma, and relativistic jet) and is beyond the scope of the present paper.

The position of the minima in the structure function is an indication of the typical timescales of the source (Nandikotkur et al. 1997). In our analysis we only found minima in the structure function of the observing block 2 (April 2008), but at different positions in SuperAGILE (16.5 days) and RXTE/ASM (6.7, 13.3, and 17.7 days). The analysis of the structure function of the Swift/BAT data in the same periods confirms the SuperAGILE minimum at 16.5 days and is accompanied by two more minima on slightly different timescales (4.9 and 11.5 days). The minima that we detected do not correspond to any known timescale of Cyg X-1, which has an orbital period of ~ 5.6 days (Lasala et al. 1998), and are not confirmed by other techniques of timing analysis. In fact, we do not detect any periodicity using the autocorrelation function, and we found only some of the timescales in the Lomb-Scargle periodogram. An inspection of the lightcurves of the OB2 reveals that the timescales found in the structure function correspond to features in the time series: 6.7 days, which is also present in the Lomb-Scargle periodogram, is the average distance between the minima in the soft X-ray lightcurve and 16.5 days is the separation of the two maxima of the emission in hard X-rays. From all these results we conclude that the timescales that we found in the structure function correspond to emission features of the specific observation period and not to general properties of the source.

6.3. The search for gamma ray emission

Thanks to the long and continuous monitoring of AGILE, we were able to investigate the possible emission of gamma rays from Cyg X-1 on both short and long timescales. An investigation on the daily timescale did not provide any significant detection. We then increased the exposure time to five days, one observing block (~ 1 month) and finally the whole 160-days observation. We did not find any signifi-

cant emission of gamma rays on any of these timescales, the typical 2σ upper limit being $\sim 100 \times 10^{-8} \text{ ph cm}^{-2} \text{ s}^{-1}$ on the one-day and $\sim 50 \times 10^{-8} \text{ ph cm}^{-2} \text{ s}^{-1}$ on the five-day timescale. The tightest 2σ upper limit derives from the integration over the whole observation (6.1 Ms net exposure) and corresponds to $\sim 5 \times 10^{-8} \text{ ph cm}^{-2} \text{ s}^{-1}$.

Recently, an episodic flare from Cyg X-1 was detected in gamma rays by AGILE in an interval of time subsequent to that considered in the present paper, and reported by Sabatini et al. (2010). Between 15 and 16 October 2009 (MJD 55119.97 – 55120.96), a flux of $(232 \pm 66) \times 10^{-8} \text{ ph cm}^{-2} \text{ s}^{-1}$ above 100 MeV was measured, at a significance level of 5.3σ pre-trial and 4σ post-trial, when the source was in a hard spectral state. Sabatini et al. (2010) also extended the search for persistent emission over all the AGILE archival data of the Cygnus Field, including the interval covered by the present paper, and did not find any significant detection. Given the longer integration time, the authors also obtained an upper limit slightly deeper than found in our analysis, $\sim 3 \times 10^{-8} \text{ ph cm}^{-2} \text{ s}^{-1}$, with an integration time of about 300 days, spread over 2.5 years.

Cyg X-1 has also been detected at TeV energies by MAGIC (Albert et al. 2007) during an \sim hour flare, at the rising edge of a flaring episode detected in both soft and hard X-rays. This rare, and so far unique, event occurred with the source in a hard spectral state, as in our observations, although reaching a flux of ~ 2 Crab in hard X-rays, while our X-ray data never show the source above 1.5 Crab. The MAGIC observation shows a power-law spectrum between 150 GeV and 2 TeV with photon index 3.2 ± 0.6 , yielding a flux of $\sim 7 \times 10^{-11} \text{ ph cm}^{-2} \text{ s}^{-1}$. If we assume that the spectrum can be extrapolated to the energy range 0.1 – 1 GeV, as when the emission site is far from the disk and the plasma, so that the cross-section of the photon conversion into electron positron pairs is negligible (see Zdziarski et al. 2009), we obtain an expected flux value of $\sim 63000 \times 10^{-8} \text{ ph cm}^{-2} \text{ s}^{-1}$. Even “diluting” such a flux on a 24-hour timescale, it would correspond to an expected day-averaged flux of $\sim 3000 \times 10^{-8} \text{ ph cm}^{-2} \text{ s}^{-1}$, well above the GRID daily sensitivity of $\sim 100 \times 10^{-8} \text{ ph cm}^{-2} \text{ s}^{-1}$. Thus, regardless of the spectral state of the source, our analysis can exclude the presence of gamma ray (GeV-)flares similar to what is observed by MAGIC at TeV energies, during the periods of the AGILE observation.

Cyg X-1 was observed by the instruments aboard the *Compton Gamma Ray Observatory* on several occasions during the first three cycles (1991 – 1994), when the source was in a low/hard state (McConnell et al. 2000). COMPTEL measured an energy spectrum described by a simple power-law with photon index 3.3 ± 0.4 , between 0.75 and 5 MeV. Above 5 MeV, the statistical quality of the data does not allow placing more than an upper limit consistent with the extrapolation of the spectrum at lower energies. During the same observations, EGRET did not detect the source, with an upper limit on the flux at $10 \times 10^{-8} \text{ ph cm}^{-2} \text{ s}^{-1}$ (100 – 200 MeV). The deepest AGILE upper limit (Sabatini et al. 2010) is about a factor of three lower than EGRET. However, an extrapolation of the COMPTEL spectrum above 100 MeV would provide an expected flux of $\sim 5 \times 10^{-9} \text{ ph cm}^{-2} \text{ s}^{-1}$, quite consistent with both of them. Our data, then, do not provide evidence of any spectral cut-off above the COMPTEL energy range.

Interestingly, Cyg X-1 was also detected by COMPTEL in high/soft state, up to about 10 MeV energy

(McConnell et al. 2002). At that time the EGRET instrument was switched off and no GeV observation is available. The COMPTEL spectrum of the soft state can be modelled with a single power-law of photon index 2.6 extending from 1 to 10 MeV. Extrapolating this energy spectrum to the AGILE energy band would provide a flux expectation of $\sim 30 \times 10^{-8} \text{ ph cm}^{-2} \text{ s}^{-1}$, easily detectable by the AGILE/GRID on a timescale of a few days. This can be seen as an additional indication that Cyg X-1 most likely remained in its low/hard spectral state during all the time of the AGILE.

The AGILE upper limits on GeV-emission from Cyg X-1 range from $100 \times 10^{-8} \text{ ph cm}^{-2} \text{ s}^{-1}$ (one day timescale) to $3 \times 10^{-8} \text{ ph cm}^{-2} \text{ s}^{-1}$ (~ 2.5 years average). Assuming a source distance of 2 kpc, (Ziółkowski 2005) they correspond to an isotropic source luminosity of $\sim 8 \times 10^{34} \text{ erg s}^{-1}$ and $\sim 2 \times 10^{33} \text{ erg s}^{-1}$, respectively. Different authors elaborated models for the high-energy emission from Cyg X-1. Zdziarski et al. (2009) proposed a model to explain the short TeV flare detected in 2006 by MAGIC (Albert et al. 2007). They propose that high-energy photons are generated by electrons accelerated to TeV energies close to the central X-ray source. The interaction of such TeV photons with the photon field of the X-ray source yields produces e^{\pm} pairs. They find that, for initial photon energies above ~ 3 TeV, photons can travel far enough, initiating extended pair cascades, in turn producing an observable flux. The predicted photon energy spectrum depends on the energy of the primary electron injection and on the stellar temperature. Under the conditions observed in X-rays during the TeV flare (when the hard X-ray flux was only \sim two times higher than what we observed with SuperAGILE, Malzac et al. 2008), the model predicts a flux in the AGILE energy range as high as $\sim 4 \times 10^{34} \text{ erg s}^{-1}$. This is a luminosity value higher than the AGILE time-averaged upper limit on the persistent emission, while it is still compatible (2 times less) with the 1-day upper limit.

Alternative models have also been proposed. Araudo et al. (2009) studied the interaction of the jet of Cyg X-1 with the wind of the companion, expected to be clumpy, and predicted the possible spectral energy distributions under different conditions of the system. Since the radiation is considered to be produced by particles accelerated in the shock due to the interaction between the jet and a cloud, the emission is predicted to be transient, with the duration timescale expected in the range between minutes to a few hours. The frequency of occurrence of such transient emission depends on the clumps’ number and size, up to appearing as a modulated steady emission. Interestingly, under some magnetic field / clump size conditions, the model predicts the radiative output due to inverse Compton effect to reach luminosities in the AGILE energy range as high as $\sim \text{few} \times 10^{34} \text{ erg s}^{-1}$, comparable to the AGILE daily upper limits and nearly one order of magnitude higher than the yearly-average limit. Also Orellana et al. (2007) suggest that the GeV – TeV emission in microquasars may originate from the interaction between the jet and the stellar wind of the companion. In this case the inelastic interactions between the relativistic protons in the jet and the cold protons of the stellar wind produce charged (π^{\pm}) and neutral (π^0) pions. The jet is assumed to be continuous and to contain a randomly oriented magnetic field. Two main channels of gamma ray production emerge from the model:

the decay of neutral pions and the emission by charged leptons, resulting from the decay of charged pions and from the photon-photon interactions, producing photons via synchrotron emission and inverse Compton scattering on the low energy stellar photons. Similar to Araudo et al. (2009), Orellana et al. (2007) present the spectral energy distribution (SED) expected in their model for the two emission channels (π^\pm and π^0) using the parameters of Cyg X-1. The gamma ray luminosity produced by the decay of the neutral pions depends on the subtended solid angle and on the inclination of the jet toward the line of sight. Taking an inclination of 30° into account (measured by Gallo et al. 2005, in radio) and a semi-opening angle of 0.1 radians, the expected luminosity is more than three orders of magnitude lower than the AGILE upper limit, at an average energy of 100 MeV. On the other hand, the leptons emitted in the decay of the charged pions can produce gamma rays via inverse Compton scattering of low energy photons from the companion star. The interactions of gamma rays with low energy photons may in turn produce relativistic e^\pm pairs that can Compton upscatter the low energy photons or trigger an electromagnetic cascade. In the SED of such secondary emission from charged pions, adopting two values of the magnetic field, 10^4 G and 10^5 G, the luminosity at 100 MeV is slightly above the $\sim 2 \times 10^{33}$ erg s $^{-1}$ AGILE upper limit for the highest magnetic field (10^5 G) while the model is still compatible with our data for a lower magnetic field, 10^4 G, whose luminosity is about one order of magnitude less than our upper limit.

7. Summary and conclusions

We reported the first campaign of observation of the hard spectral state of Cyg X-1 in gamma rays (> 100 MeV) on various timescales, with exposures ranging from one day up to ~ 160 days. We monitored the source simultaneously in hard (20 – 50 keV) and soft (2 – 12) X-rays using SuperAGILE and RXTE/ASM. The observation in hard X-rays by SuperAGILE shows the well-known erratic variability of the flux of Cyg X-1. The analysis of both the hardness ratio, estimated from the SuperAGILE flux in the two energy bands 20 – 25 keV and 25 – 50 keV, and of the colour-colour diagram, obtained from the public data of RXTE/ASM following the method reported by Reig et al. (2002), does not show any transition of spectral state. We adopted exposure times ranging from ~ 300 s up to one day and found the typical short time flickering of Cyg X-1 with intensity variations by about a factor of two.

From the study of the first-order structure function, we did not find any short lag plateau (“horizontal branch”). A power-law behaviour is found, with the Hurst exponent smaller than 0.5, denoting that the emission mechanism of Cyg X-1 is *antipersistent*, i. e. dominated by negative feedback. We also found timescales from the minima in the structure function but, from the analysis of the autocorrelation function and the Lomb-Scargle periodogram, we derive that these timescales are more probably related to particular patterns in the specific lightcurve, such as the distance between the repeated minima or the peaks of the emission, rather than to intrinsic properties of the source.

Cyg X-1 is not detected as a point like source above 100 MeV, and we find values of the upper limit ranging from $\sim 100 \times 10^{-8}$ ph cm $^{-2}$ s $^{-1}$ in one day down to

$\sim 5 \times 10^{-8}$ ph cm $^{-2}$ s $^{-1}$ for the whole observation, about a factor of two lower than from the EGRET data. We compared the luminosity derived from the AGILE upper limit above 100 MeV (assuming a distance of 2 kpc to the source) with various models of GeV – TeV emission. The predictions of the pairs’ cascade model (proposed by Zdziarski et al. 2009, to explain the TeV flaring emission detected by MAGIC) are compatible with our upper limit only for flaring emission (e. g. one-day timescale), while they are about one order of magnitude higher when compared to the year-long upper limit. We compared our results with the predictions of two alternative models, involving hadronic interactions between the cold matter of the stellar wind and the relativistic jet, proposed by Araudo et al. (2009) and Orellana et al. (2007). The first model is more suitable for flaring emission, while the second one can explain the persistent emission better. We find that the luminosity in the ~ 100 MeV range is compatible with the results of the AGILE monitoring for either short transient or for selected model parameters.

Acknowledgements. The authors are grateful to L. Stella, G. Israel, and G. Matt for useful suggestions and discussions. We also thank the anonymous referee for stimulating us to significantly improve the quality of the paper and the language editor for useful suggestions and corrections. In the paper we used the Swift/BAT transient monitor results provided by the Swift/BAT team and the RXTE/ASM public data archive. AGILE is a mission of the Italian Space Agency, with co-participation of INAF (Istituto Nazionale di Astrofisica) and INFN (Istituto Nazionale di Fisica Nucleare). This work was partially supported by ASI grants I/R/045/04, I/089/06/0, I/011/07/0 and by the Italian Ministry of University and Research (PRIN 2005025417). INAF personnel at ASDC are under ASI contract I/024/05/1.

References

- Albert, J., Aliu, E., Anderhub, H., et al. 2007, ApJ, 665, L51
- Alvarez-Ramirez, J., Cisneros, M., Ibarra-Valdez, C., & Soriano, A. 2002, Physica A Statistical Mechanics and its Applications, 313, 651
- Araudo, A. T., Bosch-Ramon, V., & Romero, G. E. 2009, A&A, 503, 673
- Belloni, T., Mendez, M., van der Klis, M., et al. 1996, ApJ, 472, L107+
- Benlloch, S., Pottschmidt, K., Wilms, J., et al. 2004, in American Institute of Physics Conference Series, Vol. 714, X-ray Timing 2003: Rossi and Beyond, ed. P. Kaaret, F. K. Lamb, & J. H. Swank, 61–64
- Brocksopp, C., Fender, R. P., Larionov, V., et al. 1999, MNRAS, 309, 1063
- Caballero-Nieves, S. M., Gies, D. R., Bolton, C. T., et al. 2009, ApJ, 701, 1895
- Cadotte, M., Sizun, P., Goldwurm, A., et al. 2006, A&A, 446, 591
- Crary, D. J., Kouveliotou, C., van Paradijs, J., et al. 1996, A&AS, 120, C153+
- Dorman, B., Arnaud, K. A., & Gordon, C. A. 2003, in Bulletin of the American Astronomical Society, Vol. 35, Bulletin of the American Astronomical Society, 641–+
- Dubus, G. 2007, arXiv:0704.0536
- Evangelista, Y., Costa, E., Del Monte, E., et al. 2006, in Society of Photo-Optical Instrumentation Engineers (SPIE) Conference Series, Vol. 6266,
- Fender, R. P., Stirling, A. M., Spencer, R. E., et al. 2006, MNRAS, 369, 603
- Feroci, M., Costa, E., Del Monte, E., et al. 2008, in Society of Photo-Optical Instrumentation Engineers (SPIE) Conference Series, Vol. 7011,
- Feroci, M., Costa, E., Del Monte, E., et al. 2010, A&A, 510, A260000+
- Feroci, M., Costa, E., Soffitta, P., et al. 2007, Nuclear Instruments and Methods in Physics Research A, 581, 728
- Frontera, F., Palazzi, E., Zdziarski, A. A., et al. 2001, ApJ, 546, 1027
- Gallo, E., Fender, R., Kaiser, C., et al. 2005, Nature, 436, 819
- Gierliński, M. & Zdziarski, A. A. 2003, MNRAS, 343, L84
- Gierliński, M., Zdziarski, A. A., Poutanen, J., et al. 1999, MNRAS, 309, 496

- Gil-Alana, L. A. 2006, *Environmental Modeling and Assessment*, 11, 19
- Gleissner, T., Wilms, J., Pooley, G. G., et al. 2004, *A&A*, 425, 1061
- Golenetskii, S., Aptekar, R., Frederiks, D., et al. 2003, *ApJ*, 596, 1113
- Herrero, A., Kudritzki, R. P., Gabler, R., Vilchez, J. M., & Gabler, A. 1995, *A&A*, 297, 556
- Holt, S. S., Kaluzienski, L. J., Boldt, E. A., & Serlemitsos, P. J. 1979, *ApJ*, 233, 344
- Horne, J. H. & Baliunas, S. L. 1986, *ApJ*, 302, 757
- Hughes, P. A., Aller, H. D., & Aller, M. F. 1992, *ApJ*, 396, 469
- Kärner, O. 2005, *Central European Journal of Physics*, 3, 190
- Koutsoyiannis, D. 2008, in *European Geosciences Union*, Vol. 10, *Geophysical Research Abstracts*
- Lasala, J., Charles, P. A., Smith, R. A. D., Balucinska-Church, M., & Church, M. J. 1998, *MNRAS*, 301, 285
- Ling, J. C., Wheaton, W. A., Wallyn, P., et al. 1997, *ApJ*, 484, 375
- Lomb, N. R. 1976, *Ap&SS*, 39, 447
- Maccarone, T. J., Coppi, P. S., & Poutanen, J. 2000, *ApJ*, 537, L107
- Makishima, K., Takahashi, H., Yamada, S., et al. 2008, *PASJ*, 60, 585
- Malzac, J., Lubiński, P., Zdziarski, A. A., et al. 2008, *A&A*, 492, 527
- Malzac, J., Petrucci, P. O., Jourdain, E., et al. 2006, *A&A*, 448, 1125
- Mason, K. O., Hawkins, F. J., Sanford, P. W., Murdin, P., & Savage, A. 1974, *ApJ*, 192, L65+
- McConnell, M. L., Ryan, J. M., Collmar, W., et al. 2000, *ApJ*, 543, 928
- McConnell, M. L., Zdziarski, A. A., Bennett, K., et al. 2002, *ApJ*, 572, 984
- Mirabel, I. F. & Rodríguez, L. F. 1999, *ARA&A*, 37, 409
- Nandikotkur, G., Sreekumar, P., & Carter-Lewis, D. A. 1997, in *American Institute of Physics Conference Series*, Vol. 410, *Proceedings of the Fourth Compton Symposium*, ed. C. D. Dermer, M. S. Strickman, & J. D. Kurfess, 1361–1365
- Neronov, A., Bel, M. C., Shaw, S., et al. 2008, *The Astronomer's Telegram*, 1533, 1
- Orellana, M., Bordas, P., Bosch-Ramon, V., Romero, G. E., & Paredes, J. M. 2007, *A&A*, 476, 9
- Paltani, S., Courvoisier, T., Blecha, A., & Bratschi, P. 1997, *A&A*, 327, 539
- Pottschmidt, K., Wilms, J., Chernyakova, M., et al. 2003, *A&A*, 411, L383
- Priedhorsky, W. C., Brandt, S., & Lund, N. 1995, *A&A*, 300, 415
- Reig, P., Papadakis, I., & Kylafis, N. D. 2002, *A&A*, 383, 202
- Rico, J. 2008, *ApJ*, 683, L55
- Rutman, J. 1978, in *Proceedings of the IEEE*, Vol. 66, *Proceedings of the IEEE*, ed. , 1048–1075
- Sabatini, S., Tavani, M., Striani, E., et al. 2010, *ApJ*, 712, L10
- Scargle, J. D. 1982, *ApJ*, 263, 835
- Shaposhnikov, N. & Titarchuk, L. 2007, *ApJ*, 663, 445
- Simonetti, J. H., Cordes, J. M., & Heeschen, D. S. 1985, *ApJ*, 296, 46
- Stirling, A. M., Spencer, R. E., de la Force, C. J., et al. 2001, *MNRAS*, 327, 1273
- Tavani, M., Barbiellini, G., Argan, A., et al. 2008, *Nuclear Instruments and Methods in Physics Research A*, 588, 52
- Vercellone, S., Chen, A. W., Giuliani, A., et al. 2008, *ApJ*, 676, L13
- Zdziarski, A. A. & Gierliński, M. 2004, *Progress of Theoretical Physics Supplement*, 155, 99
- Zdziarski, A. A., Malzac, J., & Bednarek, W. 2009, *MNRAS*, 394, L41
- Zdziarski, A. A., Poutanen, J., Paciesas, W. S., & Wen, L. 2002, *ApJ*, 578, 357
- Ziółkowski, J. 2005, *MNRAS*, 358, 851

Table 1. The observation log

Obs. period	Date	Modified Julian Day	off-axis angle [degrees]	exposure [ks]
OB1	02 Nov 2007 13:50 UT – 16 Dec 2007 10:27 UT	54406.576 – 54450.435	2.4 – 27.6	1634
OB2	10 Apr 2008 15:10 UT – 30 Apr 2008 11:15 UT	54566.632 – 54586.469	18.3 – 15.4	893
OB3	10 May 2008 17:52 UT – 30 Jun 2008 11:10 UT	54596.744 – 54647.465	4.6 – 32.7	1934
OB4	17 Oct 2008 17:00 UT – 01 Dec 2008 11:37 UT	54756.708 – 54801.484	15.1 – 18.0	1632

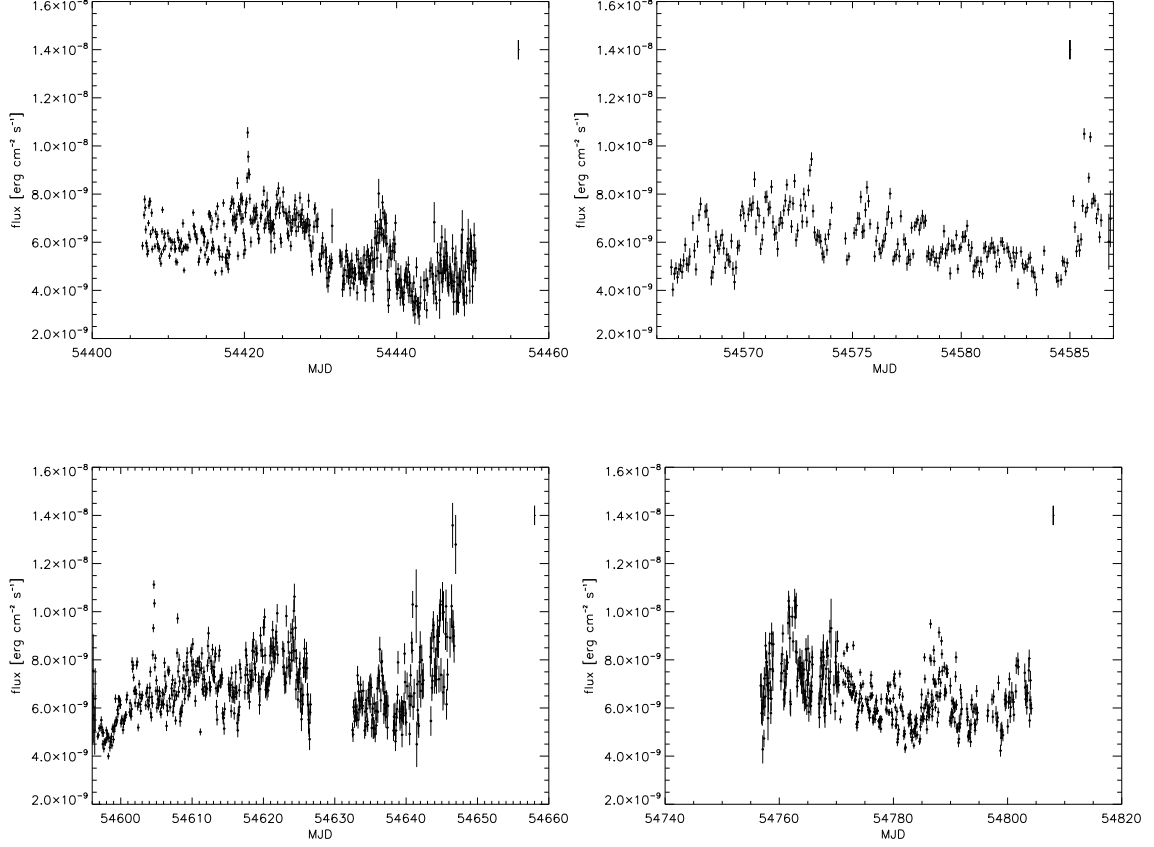


Fig. 3. SuperAGILE lightcurve of Cyg X-1 during the observing periods 1 (top left), 2 (top right), 3 (bottom left) and 4 (bottom right). Each point represents the normalized rate estimated in one satellite orbit (with exposure of ~ 3 ks). The normalized rate values are converted into units of $\text{erg cm}^{-2} \text{s}^{-1}$ considering the source average spectrum. Only the statistical uncertainty is shown on the points in the plots. The average systematic uncertainty on the flux calibration is plotted in the top right angle of each plot.

Table 2. Parameters of the spectral fit of Cyg X-1. χ_r^2 is the reduced chi square, the uncertainties are at 90 % confidence level and include a 5 % systematic error.

Normalized rate [cts $\text{cm}^{-2} \text{s}^{-1}$]	photon index	flux [$\text{erg cm}^{-2} \text{s}^{-1}$]	χ_r^2	degrees of freedom
0.12	$1.63^{+0.09}_{-0.08}$	$(7.6 \pm 0.3) \times 10^{-9}$	1.159	31
0.17	1.60 ± 0.11	$(8.3 \pm 0.4) \times 10^{-9}$	1.113	32
0.08	1.74 ± 0.09	$(4.6 \pm 0.4) \times 10^{-9}$	0.986	29

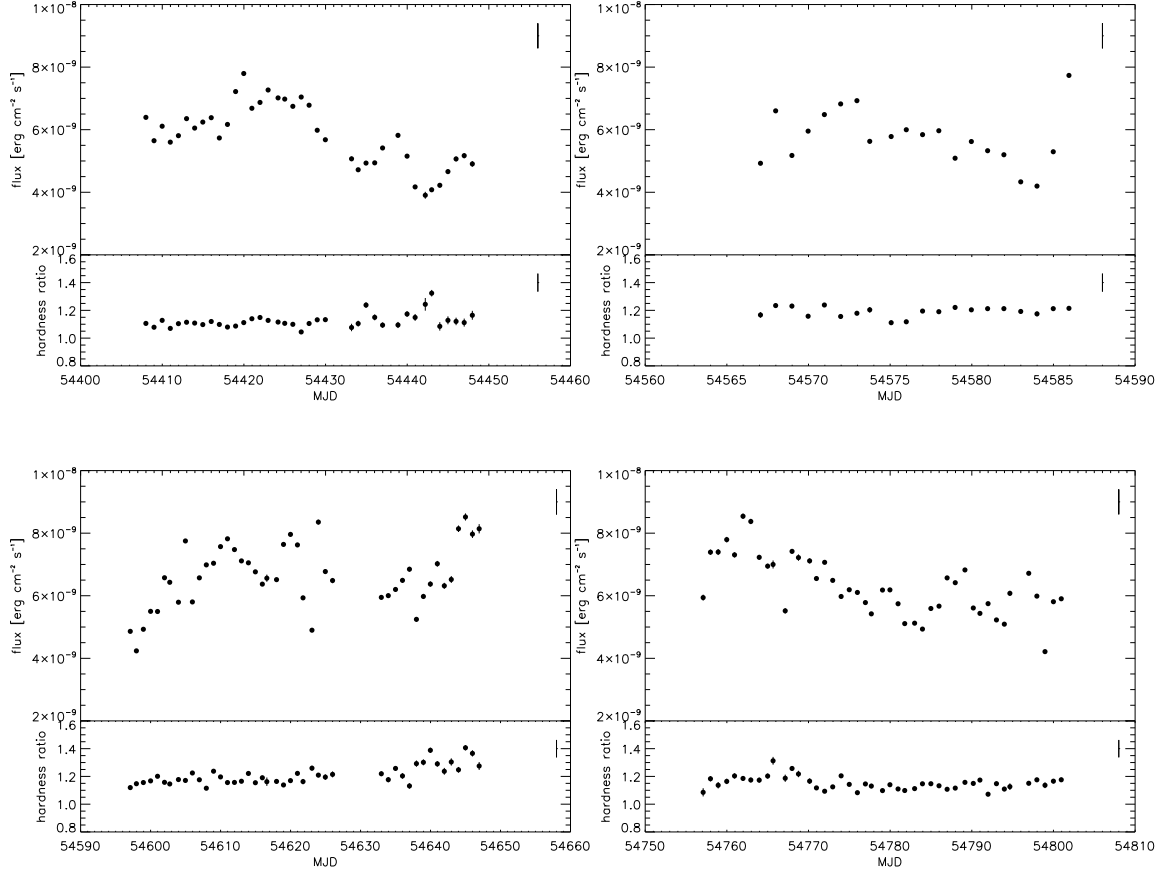


Fig. 6. SuperAGILE daily lightcurve of Cyg X-1 during the observing blocks 1 (top left), 2 (top right), 3 (bottom left), and 4 (bottom right). Each point represents the normalized rate estimated in one day (with exposure of ~ 40 ks). The rate values are converted into units of $\text{erg cm}^{-2} \text{s}^{-1}$ considering the source average spectrum. The hardness ratio is computed as the ratio of the emission in the HE band ($25 - 50$ keV) to the LE one ($20 - 25$ keV). Only the statistical uncertainty is shown on the points in the plots. The average systematic uncertainty is plotted in the top right corner of each plot.

Table 3. Analysis of the structure function in the hard X-ray band

Obs. period	start lag [s]	end lag [s]	H
OB1	$10^{4.9}$	10^6	0.185
OB2	$10^{3.9}$	$10^{5.2}$	0.147
OB3	$10^{3.9}$	$10^{4.9}$	0.115
	$10^{5.2}$	$10^{5.6}$	0.210
OB4	$10^{4.9}$	$10^{5.7}$	0.170

Table 4. Analysis of the structure function in the soft X-ray band

Obs. period	start lag [s]	end lag [s]	H
OB1	$10^{3.7}$	$10^{4.7}$	0.144
	$10^{5.2}$	10^6	0.186
OB2	10^4	$10^{5.2}$	0.148
OB3	$10^{4.2}$	$10^{5.2}$	0.066
OB4	$10^{4.2}$	$10^{5.2}$	0.050

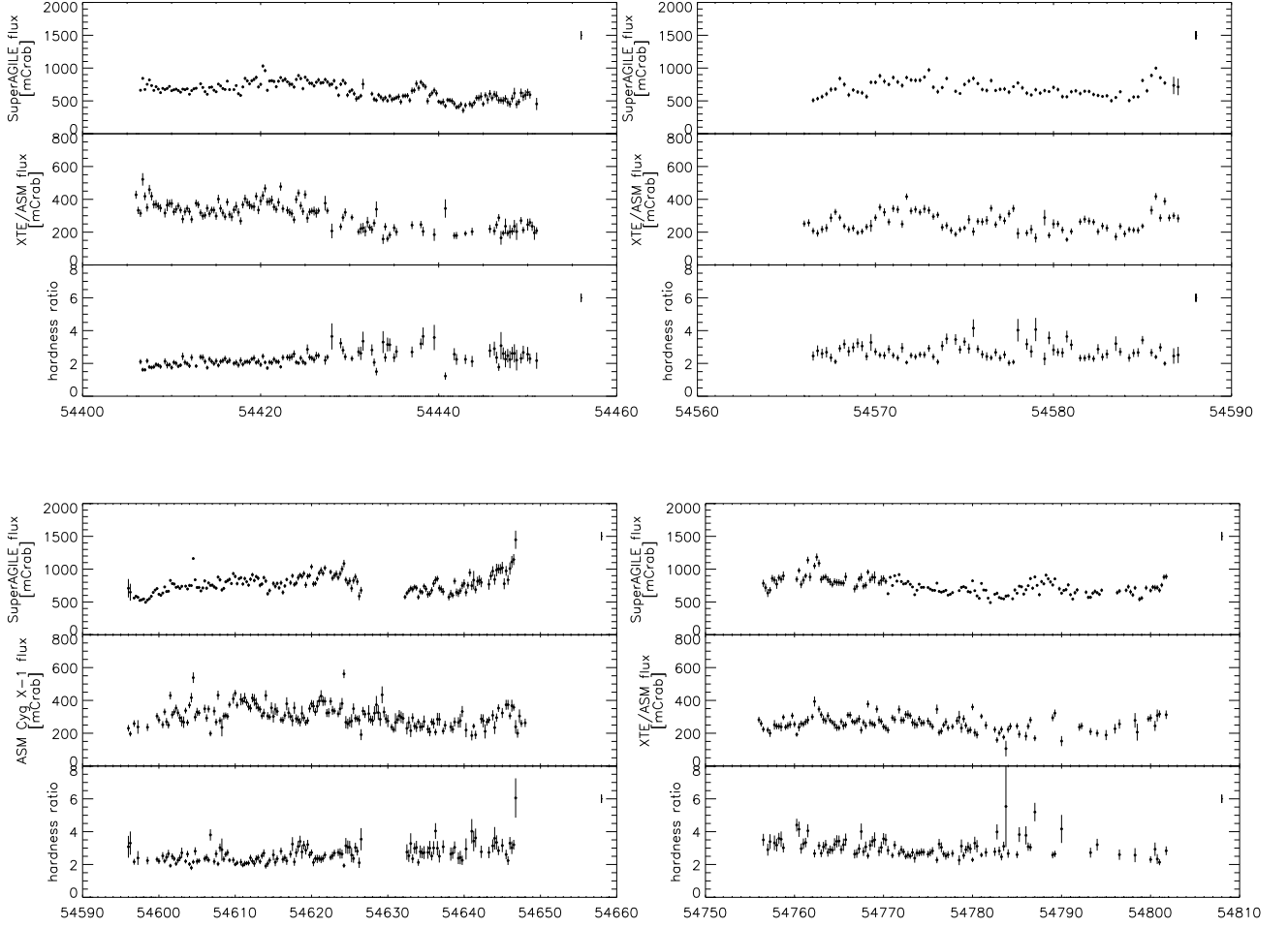


Fig. 7. Superposition of the SuperAGILE (top panels) and RXTE/ASM (middle panels) lightcurves of Cyg X-1 and hardness ratio (bottom panels) during the observing periods 1 (top left), 2 (top right), 3 (bottom left), and 4 (bottom right). The arrows show the position of periods of increase in the source emission that are visible in the hard X-ray band but not in the soft one. Both lightcurves in each period are accumulated on the same time interval with a bin size of six hours. Only the statistical uncertainty is shown on the points in the plots of the SuperAGILE flux and of the hardness ratio. The average systematic uncertainty is plotted in the top right corner of each plot.